MULTI-ANGLE TOF MR BRAIN ANGIOGRAPHY OF THE COMMON MARMOSET

M. Mescam, J. Brossard, N. Vayssière and C. Fonta

CNRS CERCO UMR5549, Toulouse, France

ABSTRACT

The relation between normal and pathological aging and the cerebrovascular component is still unclear. In this context, the common marmoset, which has the advantage of enabling longitudinal studies over a reasonable timeframe, appears as a good pre-clinical model. However, there is still a lack of quantitative information on the macrovascular structure of the marmoset brain. In this paper, we investigate the potentiality of multi-angle TOF MR angiography using a 3T MRI scanner to perform morphometric analysis of the marmoset brain vasculature. Our image processing pipeline greatly relies on the use of multiscale vesselness enhancement filters to help extract the 3D macrovasculature and perform subsequent morphometric calculations. Although multi-angle acquisition does not improve morphometric analysis significantly as compared to single-angle acquisition, it improves the network extraction by increasing the robustness of image processing algorithms.

***Index Terms*—** Non-human primate, brain, vessels, MRI, morphometry

1. INTRODUCTION

Population aging leads to a crucial need for a better understanding of the role of the vascular component, not only in normal brain aging, but also in the development and evolution of neurovascular and neurodegenerative diseases [1]. This requires studying the evolution with age, or with the stage of a pathology, of the cerebral vascular system and its interactions within the whole cardiovascular system.

In this context, we need good pre-clinical models that we can follow longitudinally over reasonable time scales. Non-human primates are usually preferred to rodents or to other mammals because of their phylogenetic proximity to humans. More specifically, the common marmoset monkey (*Callithrix jacchus*), which has been increasingly studied over the past years in the field of brain sciences, has proven to be a good candidate for longitudinal studies, with an average lifespan of $\sim$10 years in captivity [2]. The cerebral microvascularization of the marmoset has been studied post-mortem in the brain cortex with X-ray microtomography [3,4]. However, as far as we know, there is no quantitative analysis of the morphometry of the marmoset whole brain macrovasculature.

Compared to high-resolution techniques such as X-ray microtomography, often performed post-mortem, Time Of Flight MR Angiography (TOF MRA) provides a non invasive way to access and as importantly to follow the evolution of the vasculature topology, geometry and morphometry without the use of contrast agents. Contrast between vessels and surrounding tissues in the image is obtained by performing MRI acquisition perpendicularly to fluid flow. It is thus crucial to optimize the angle of acquisition with respect to the flow direction in order to visualize the vessels of interest.

However, imaging small animals like the marmoset, poses additional challenges: images are either obtained with a high-field MRI scanner (4.7T and above), with associated artefacts such as field inhomogeneity, or with less adapted, but more easily available clinical scanners originally dedicated to human research. In the latter case, the compromise between image resolution and signal-to-noise ratio (SNR) is more critical and it becomes crucial to apply adequate processing algorithms in order to recover the original information among noise. Vesselness enhancement filters have been specifically developed for applications like MRA, in order to extract tubular structures, typically vascular information, from noisy data [5–9].

Here, TOF MRA was tested using a multi-angle approach in order to improve image analysis. The acquisitions were rigidly aligned and merged, and the resulting 3D image was pre-processed using multiscale vesselness enhancement filters adapted from [5] and [6]. The enhanced images were finally segmented and diameters of extracted vessels were computed using a skeletonization approach.

2. MATERIALS & METHODS

2.1. Image acquisition

Acquisitions were performed on a 3T Philips MRI scanner dedicated to human and large animal research. As mentioned above, using such device for small animal reseach is challenging and necessitates optimized protocols in order to obtain the most precise images in terms of spatial resolution and SNR. Here, Time Of Flight (TOF) MR angiography was performed on a 6-year-old marmoset using a Fast Field Echo se-

Thanks to IDEX program of the University of Toulouse for funding.

quence (acquisition parameters: TR = 25ms, TE = 3.454 ms, flip angle = 20°, slice thickness = 0.8 mm and reconstruction voxel size = 0,29× 0.29×0.4 mm^3). During the whole acquisition process, the animal was anaesthesized and monitored for cardiac rythm and blood oxygenation[1].

In TOF imaging, when a vessel crosses the acquisition slice, signal intensity in a corresponding voxel depends on the flow velocity. Ideally, *i.e.* when the vessel crosses the slice perpendicularly, the real inner section of the tube is then visible on the resulting image. However, tortuosity and multidirectional paths of vessels make it impossible to capture the whole vessel population within one acquisition. Since we are interested in morphometric aspects of the vasculature, we investigate in this paper the influence of the number of acquisition angles on the quality of the final segmentation, and more specifically on resulting measured diameters. One clearly identified limit of this approach is the total available acquisition time, which is conditioned by the anaesthesia. Besides, a precise morphometry analysis relies upon the quality of the image in terms of spatial resolution as well as SNR, which also condition the time required for each acquisition. Based on those considerations, four acquisitions were added, corresponding to four regularly distributed angles ($-40°$, $-20°$, $+20°$, $+40°$), with respect to the $0°$ angle as the routinely used acquisition plane, *i.e.* approximately perpendicularily to the carotids (Fig.1). Although we focused our interest primarily on the arterial network, note that the same technique could be applied for imaging the cerebral venous system, by choosing accordingly the acquisition orientation.

2.2. Image processing

2.2.1. Image registration

Images obtained at various angles were rigidly aligned using the software Avizo[2]. This process does not involve any nonlinear transformation since we are performing intra-subject unimodal registration. In that case, normalized cross-correlation, calculated upon intensity values in grey level images, appeared to be an appropriate objective function. In order to limit errors due to resampling approximations, the middle image (angle 0°) was used as the reference image. In addition, three interpolation methods were tested for the resampling task and compared: nearest-neighbor, trilinear and B-splines interpolations. Finally, all the registered volumes were merged into a single 3D volume by voxel averaging.

2.2.2. Vessel enhancement

A critical but necessary step prior to extracting the vasculature from the 3D volume, consists in enhancing the signal in vessels compared to surrounding tissues.

In our images, vessels mostly have tubular structures, with signal intensity close to white matter intensity, and are characterized by small diameters (< 2 mm) [10].

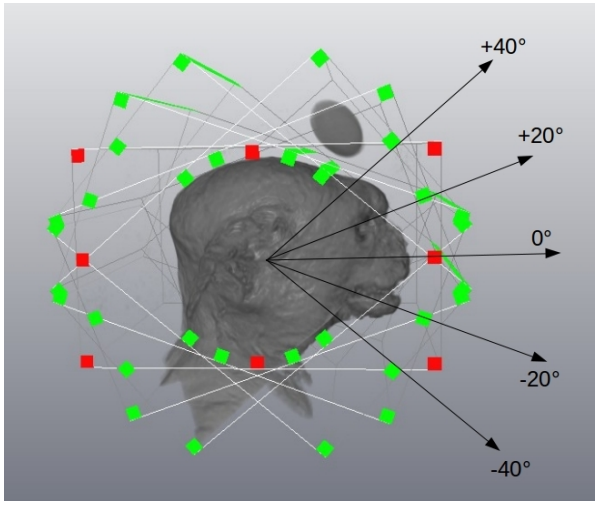

Fig. 1. 3D volume rendering of the merged MRI images, along with their acquisition boxes, corresponding to five different angles with respect to the chosen reference acquisition plane, perpendicular to the carotids ($0°$).

Several Hessian-based filters have been developed in the past, to enhance vessels from surrounding tissues based on their tubular shape. Among them, Sato [5] and Frangi [6] filters automatically track network centerlines by tweaking the eigenvalues of the Hessian matrix of the image intensity map. We have tested and compared those two algorithms. In both cases, the first step consisted in applying a multiscale gaussian filter G to the raw image I with an iteratively increasing kernel size σ ranging from 0.1 to 0.9 with a 0.1 step (1-2).

$$G(x,y,z,\sigma) = \frac{1}{(\sigma\sqrt{2\pi})^3}.e^{-\frac{x^2+y^2+z^2}{2\sigma^2}} \quad (1)$$

$$\tilde{I}(x,y,z,\sigma) = G(x,y,z,\sigma) * I(x,y,z) \quad (2)$$

$$\tilde{H}(x,y,z,\sigma) = \begin{pmatrix} \frac{\partial^2 \tilde{I}}{\partial x^2} & \frac{\partial^2 \tilde{I}}{\partial x \partial y} & \frac{\partial^2 \tilde{I}}{\partial x \partial z} \\ \frac{\partial^2 \tilde{I}}{\partial y \partial x} & \frac{\partial^2 \tilde{I}}{\partial y^2} & \frac{\partial^2 \tilde{I}}{\partial y \partial z} \\ \frac{\partial^2 \tilde{I}}{\partial z \partial x} & \frac{\partial^2 \tilde{I}}{\partial z \partial y} & \frac{\partial^2 \tilde{I}}{\partial z^2} \end{pmatrix} \quad (3)$$

Given λ_1, λ_2 and λ_3 the eigenvalues of the Hessian $\tilde{H}$ (3), an ideal tubular structure should verify (4):

$$\begin{cases} |\lambda_1| \approx 0 \\ |\lambda_1| \ll |\lambda_2| \\ |\lambda_2| \approx |\lambda_3| \end{cases} \quad (4)$$

However vessels are not ideal tubes, and the filters cited above use different tubularity, or vascularity criteria (5-6).

$$f_{\text{sato}} = \begin{cases} \sigma^2|\lambda_3|\left(\left|\frac{\lambda_2}{\lambda_3}\right|\right)^{\lambda_{23}}\left(1+\frac{\lambda_1}{|\lambda_2|}\right)^{\lambda_{12}} & \text{if } \lambda_1 \leq 0 \\ \sigma^2|\lambda_3|\left(\left|\frac{\lambda_2}{\lambda_3}\right|\right)^{\lambda_{23}}\left(1+\alpha\frac{\lambda_1}{|\lambda_2|}\right)^{\lambda_{12}} & \text{if } 0 < \lambda_1 \leq \frac{|\lambda_2|}{\alpha} \\ 0 \quad \text{else} \end{cases} \quad (5)$$

[1]Government authorization from the MENESR (project #05215.03)

[2]www.fei.com/software/amira-avizo

$$f_{\text{frangi}} = \begin{cases} 0 \quad \text{if } \lambda_2 > 0 \text{ or } \lambda_3 > 0 \\ \left(1 - e^{-\frac{R_A^2}{2a^2}}\right) e^{-\frac{R_B^2}{2b^2}} \left(1 - e^{-\frac{S^2}{2c^2}}\right) \text{ else} \end{cases} \quad (6)$$

where $R_A = \frac{|\lambda_2|}{|\lambda_3|}$, $R_B = \frac{|\lambda_1|}{|\lambda_2 \lambda_3|}$ and $S = \sqrt{\lambda_1^2 + \lambda_2^2 + \lambda_3^2}$. In both cases, geometrical and contrast properties are controlled by adjustable parameters: α, λ_{12} and λ_{23} for Sato filter and a, b and c for Frangi filter.

2.2.3. Vessel segmentation and morphometry

The final processing step consisted in segmenting the enhanced image in order to extract the vascular structure as one single object, further dedicated to topological or morphometrical analysis (*e.g.* diameters). This was achieved here by semi-automatic thresholding (using appropriate values in Avizo). Vessel diameters were automatically computed in Avizo using a skeletonization process. More precisely, the local thickness was computed in each voxel of the segmented object, as the diameter of the largest ball entirely included in the object (vessel), and containing the voxel.

3. RESULTS

Contrarily to single-angle TOF MRA, whose resulting image can be used directly as an input in filtering and segmentation algorithms, multi-angle TOF MRA requires a prior registration step. Even though here we are dealing with rigid unimodal registration, this added step involves image resampling, which may have degrading effects on the image, especially when voxels are not perfectly isotropic. As mentioned in section 2.2.1, we tested three interpolation methods. We retained, for subsequent analysis, the trilinear interpolation method, which induced less aliasing and distorsion artefacts than the nearest-neighbor and B-splines interpolation methods (data not shown). A volume rendering of the 3D merged registered images is shown in Fig.1, and a Maximum Intensity Projection in the coronal plane is shown in Fig.2a.

Contrast enhancement between vessels and surrounding tissues was tested with Sato filter and Frangi filter, two multiscale filters specifically designed to enhance tubular structures such as vessels, as described in section 2.2.2. Both models were parameterized so as to be adapted to our images, and more particularly to the order of magnitude of macrovessels' diameters in the marmoset brain. A multiscale smoothing was first performed on the 3D raw image according to (1). Parameters related to geometrical properties of the tubular shape or to the grey level intensity contrast were manually adjusted based on visual inspection. The optimal sets of parameters were $[\alpha = 0.02,\ \lambda_{12} = 2,\ \lambda_{23} = 1]$ for the Sato vascularity criterion (5), and $[a = 0.1,\ b = 0.5,\ c = 70]$ for the Frangi vascularity criterion (6). Coronal projections of the corresponding filtered volumes are shown in Fig.2b-c.

Following noise reduction and vessel enhancement, the images were segmented in order to extract the 3D vasculature.

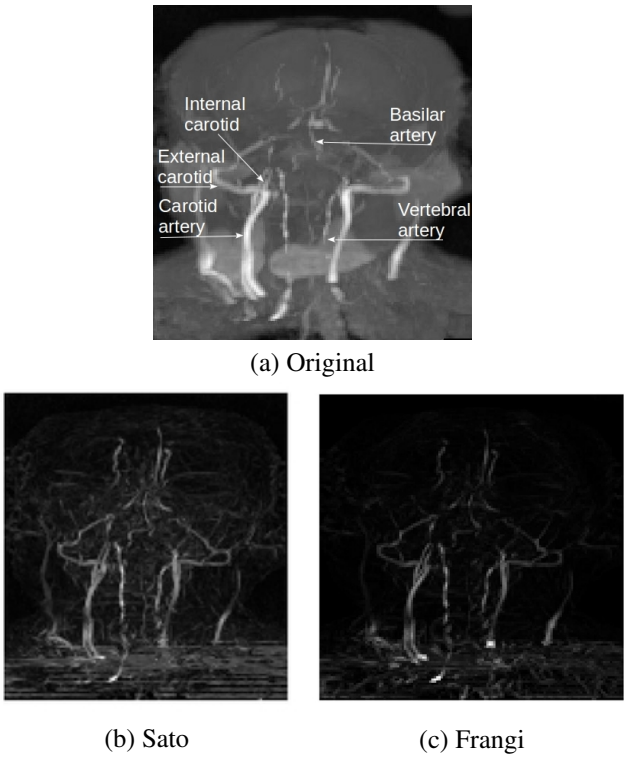

(a) Original

(b) Sato (c) Frangi

Fig. 2. (a) Initial registered and merged 3D image of the marmoset head shown in the coronal plane (voxel size $0.29 \times 0.29 \times 0.4$ mm^3). Same image after vessel enhancement using (b) Sato vesselness filter and (c) Frangi vesselness filter.

Finally, diameters were computed using a skelotonization approach. A 3D representation of the vascular structure segmented with the thresholding method is given in Fig.3 with a color code for diameter. Vessel diameters ranged from 0.2 to 1.16mm for the 3D structure obtained from both single-angle and multi-angle acquisitions.

4. DISCUSSION & CONCLUSION

Longitudinal studies of the macrovascular system relies upon the extraction of the 3D brain vasculature, along with an accurate characterization of its topology and morphometry. Because they are routinely used in clinics and in human research, 3T MRI scanners are also more accessible for small animal research than higher field devices.

In this paper, we show the potentiality of multi-angle TOF MRA using a 3T MRI scanner to analyze the marmoset brain vasculature. We provide qualitative comparisons of image acquisition and processing techniques in order to define an adequate pipeline for morphometric analysis. Measured diameters are in agreement with values reported in [10], with for instance values around 0.5 mm for vertebral arteries and closer to 1 mm for carotids. At the acquisition level, we observe that merging several images acquired with different angles does

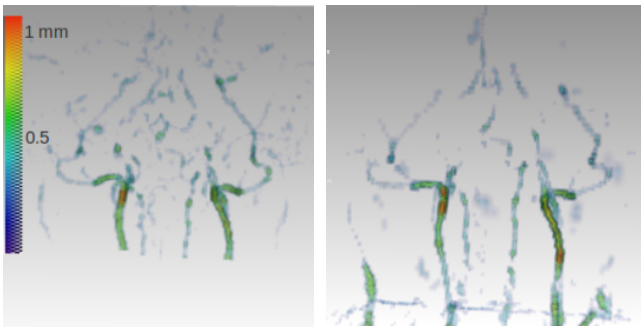

(a) Single angle (b) Multi-angle

Fig. 3. 3D representation of the segmented vasculature, color-coded for diameter.

not increase significantly the precision of morphometric analysis for easily detected vessels. Indeed, diameter values are in the same range regardless of the acquisition protocol (Fig.3a-b). However, qualitative assessment shows that, as expected, more structures are detected and vessels present less discontinuities with multi-angle acquisition, which leads to a more efficient filtering and consequently to a better segmentation.

Note that even with an optimized acquisition procedure, powerful post-processing algorithms are needed in order to recover the true information among noise. At the image processing level, noise removal is a critical step towards a good morphometric analysis: on the one hand, a weak filtering leads to incorrect estimations, as noise and/or surrounding structures are wrongly attributed to vessels. On the other hand, over-filtering may cause vessel segment fragmentation, thinning or suppression, leading to underestimated vessel diameters. We have shown that the typically used Frangi filter performs better than Sato filter to enhance the vessels in our images, although this can still be improved. It will be worth testing other existing structure enhancers, for instance based on the Optimally Oriented Flux (OOF) [11], or on recently developed morphological paths operators [12]. Another future prospect concerns the adaptation or development of more advanced semi-automatic segmentation methods, such as level-sets or graphcuts-based approaches, which have already proven to be efficient on human brain MR angiography. Furthermore, manual segmentations by experts will serve as ground truth for quantitative validation of the proposed acquisition, filtering and segmentation approaches.

To the best of our knowledge, this is the first non-invasive quantitative analysis of the brain macrovasculature in the marmoset monkey. Such information can further be used to parameterize and validate blood flow models, therefore helping us gain insight into the mechanisms of brain aging.

5. ACKNOWLEDGMENT

We thank A. Sadoun for his expertise in neuroanatomy, the CerCo animal rearing facilities for their help with animal preparation, as well as the MRI platform of INSERM TONIC UMR1214 and more particularly J.-P. Desirat and Y. Fave, for their help with image acquisition.

6. REFERENCES

[1] Ungvari Z. and Sonntag W.E., "Brain and cerebrovascular aging - new mechanisms and insights," *J Gerontol A Biol Sci Med Sci*, vol. 69, pp. 1307–1310, 2014.

[2] Tardif S.D., Mansfield K.G., Ratnam R, Ross C.N., and Ziegler T.E., "The marmoset as a model of aging and age-related diseases," *Institute for Laboratory Animal Research J*, vol. 52, pp. 54–65, 2011.

[3] Risser L., Plouraboué F., Cloetens P., and Fonta C., "A 3d-investigation shows that angiogenesis in primate cerebral cortex mainly occurs at capillary level," *Int J Dev Neurosci*, vol. 27, pp. 185–196, 2009.

[4] Guibert R., Fonta C., and Plouraboué F., "Cerebral blood flow modeling in primate cortex," *J Cereb Blood Flow Metab*, vol. 30, pp. 1860–1873, 2010.

[5] Sato Y., Nakajima S., Shiraga N., Atsumi H., Yoshida S., Koller T., Gerig G., and Kikinis R., "Three-dimensional multi-scale line filter for segmentation and visualization of curvilinear structures in medical images," *Med Image Anal*, vol. 2, pp. 143–168, 1998.

[6] Frangi A.F., Niessen W.J., Vincken K.L., and Viergever M.A., "Multiscale vessel enhancement filtering," *In: MICCAI'98; Lecture notes in computer science. Berlin: Springer*, p. 130137, 1998.

[7] Erdt M., Raspe M., and Suehling M., "Automatic hepatic vessel segmentation using graphics hardware," *In: MIAR'08; Lecture notes in computer science. Berlin: Springer*, pp. 403–412, 2008.

[8] Shikata H., McLennan G., Hoffman E.A., and Sonka M., "Segmentation of pulmonary vascular trees from thoracic 3d ct images," *Int J Biomed Imaging*, vol. doi:10.1155/2009/636240, 2009.

[9] Hsu C.Y., Schneller B., Alaraj A., Flannery M., Zhou X.J., and Linninger A., "Automatic recognition of subject-specific cerebrovascular trees," *Magn Reson Med*, vol. DOI:10.1002/mrm.26087, 2016.

[10] Virley D., Hadingham S.J., Roberts J.C., Farnfield B., Elliott H., Whelan G., Golder J., David C., Parsons A.A., and Hunter A.J., "A new primate model of focal stroke: endothelin-1-induced middle cerebral artery occlusion and reperfusion in the common marmoset," *J Cereb Blood Flow Metab*, vol. 24, pp. 24–41, 2003.

[11] Law M.L. and Chung A.C., "Three dimensional curvilinear structure detection using optimally oriented flux.," *In: ECCV'08; Lecture notes in computer science. Berlin: Springer*, pp. 368–382, 2008.

[12] Merveille O., Talbot H., Najman L., and Passat N., "Tubular structure filtering by ranking orientation responses of path operators," *In: ECCV'14; Lecture notes in computer science. Berlin: Springer*, pp. 203–218, 2014.